Scripta Materialia 268 (2025) 116878

Contents lists available at ScienceDirect

Scripta Materialia

journal homepage: www.journals.elsevier.com/scripta-materialia

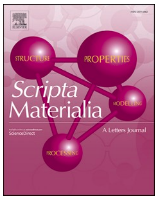

Structural origin of hot-compression-enhanced mechanical properties of aluminosilicate glass

Ziming Yan [a], Zhen Zhang [b], Madoka Ono [c], Juanjuan Zhu [a], Linfeng Ding [a,*], Lianjun Wang [a]

[a] State Key Laboratory of Advanced Fiber Materials, College of Materials Science and Engineering, Engineering Research Center of Advanced Glass Manufacturing Technology, Ministry of Education, Donghua University, Shanghai 201620, China
[b] College of Physics, Chengdu University of Technology, Chengdu 610059, China
[c] Department of Applied physics, Graduate School of Engineering, Tohoku University, Sendai, Miyagi 980-8579, Japan

ARTICLE INFO

Keywords:
Oxide glass
Hot-compression
Atomic structure
Mechanical properties
Molecular dynamics simulations

ABSTRACT

Hot-compression treatment has emerged as an effective method for improving mechanical properties of oxide glasses. However, the pressure-induced structural changes that are responsible for the enhanced mechanical properties have remained elusive. Using molecular dynamics simulations, we find that increasing pressure significantly improves the fracture toughness and nano-ductility of a calcium aluminosilicate, consistent with experiments. The enhanced mechanical properties can be traced back to the increase of atomic coordination numbers, decrease of oxygen-centered bond angles, as well as reorganization of medium-range structure as seen from the change of network topology. Moreover, our simulations highlight oxygen tri-clusters ($^{(3)}$O) as critical sites for enhancing fracture toughness and nano-ductility, as they are active for dynamic bond rupturing and reformation. These findings help to understand how hot compression alters the structure and mechanical properties of oxide glasses, insights that are crucial for improving mechanical performance of network-forming materials.

Alkali and alkaline earth aluminosilicate glasses have become important materials in many industrial and technological applications, such as nuclear waste storage [1,2], touchscreens [3,4], and liquid crystal display substrates [5,6]. The introduction of Al_2O_3 plays a crucial role in improving the chemical durability, mechanical properties, and various thermodynamic behaviors of the glass. For example, Yoshida et al. [7] showed that with an increase in Al_2O_3 content, the rigidity of sodium aluminosilicate glass was enhanced, which increased the likelihood of crack initiation and reduced the crack initiation load. Ke et al. [8] found that increasing the alumina-to-silica ratio in magnesium aluminosilicate glass significantly improved the hardness and crack resistance of the glass.

In addition to composition, temperature and pressure are also two additional effective ways to control glass structure and tailor glass properties, including not only optical transparency [9,10], but also mechanical performance. For instance, Guerette et al. [11] demonstrated that under high-temperature (1100 °C) and high-pressure (8 GPa) conditions, the density of silicate glass increased by about 25 %, and the Young's modulus increased by about 71 %. Lee et al. [12] observed that hot-compression treatment can promote the densification of borosilicate glass, thereby improving its Young's modulus and fracture toughness. Notably, based on the discovery of quasicrystalline materials with medium-range order [13].A recent study [14] have found that $3CaO\text{-}Al_2O_3\text{–}3SiO_2$ glass, under high-temperature (1000 °C) and high-pressure (15 GPa) annealing treatment, forms a paracrystalline structure inside, significantly improving its fracture toughness, reaching up to 1.99 ± 0.06 MPa·m$^{1/2}$, surpassing all known oxide glasses. These results indicate that the structural changes in glass caused by thermal and pressure treatments are not only significant but also extremely complex, further highlighting the importance of gaining a deeper understanding of the internal structural changes for developing glasses with better performance.

Therefore, in this work we focus on the $3CaO\text{-}Al_2O_3\text{–}3SiO_2$ system, with the best fracture toughness on record among all known oxide glasses [14], and extensively investigate the effects of hot-compression treatment at different pressures on the glass structure and properties through molecular dynamics simulations. These microscopic insights are crucial for understanding the structural response of aluminosilicate glasses under pressure and improving their mechanical properties.

Classical molecular dynamics (MD) simulations were performed on

---

* Corresponding author.
E-mail address: Linfeng.Ding@dhu.edu.cn (L. Ding).

https://doi.org/10.1016/j.scriptamat.2025.116878
Received 23 May 2025; Received in revised form 8 July 2025; Accepted 9 July 2025

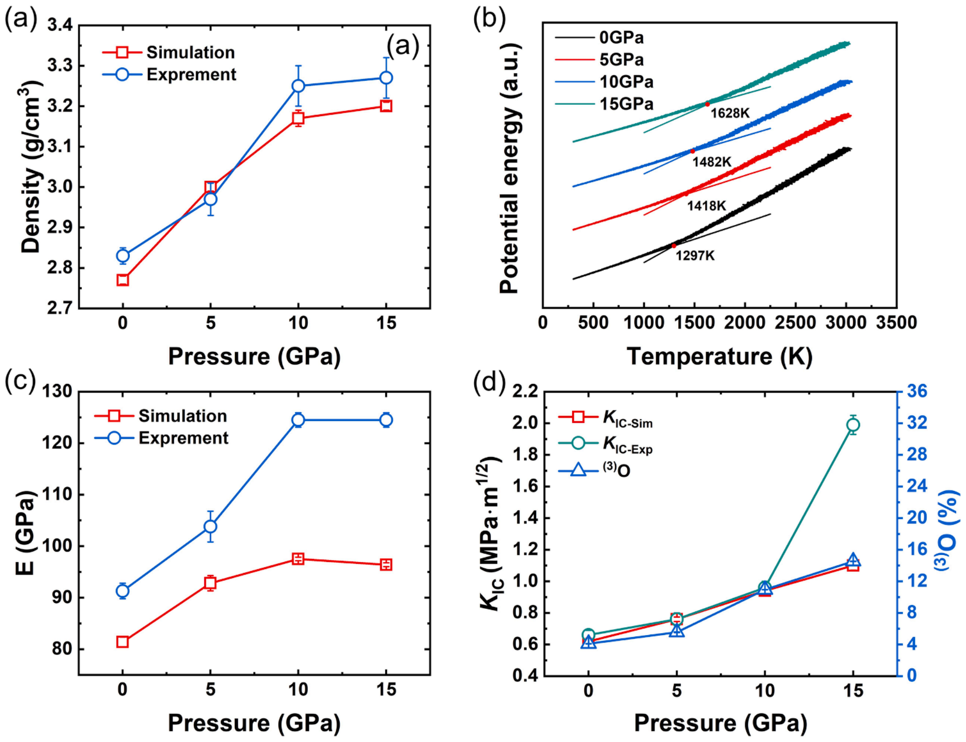

Fig. 1. The distribution of (a) density, (b) glass transition temperature (Curves with different pressures are shifted in the y-axis for clarity.), (c) Young's modulus, (d) fracture toughness and oxygen tri-clusters under different pressures.

the 3CaO-Al_2O_3–$3SiO_2$ (hereafter denoted as CAS) glass system. The simulation used the two-body effective potential (SHIK potential) recently developed by Sundararaman et al. [15–17], which has been demonstrated to reliably describe the structural, mechanical, and surface properties of multicomponent silicate glasses [18–20]. The key steps for preparing glass samples by conventional melt-quenching methods are as follows: First, 5000 atoms are randomly inserted into a cubic simulation box (4 × 4 × 4 nm^3), with an initial density of 2.83 g/cm^3 (as measured experimentally). The sample undergoes a melt-equilibration process at 3000 K, followed by cooling to 300 K at a rate of 1 K/ps and relaxing for 125 ps at 300 K. The entire process is carried out in an NPT ensemble under zero pressure conditions, with periodic boundary conditions applied in all directions. This whole melt-quenching procedure has been fully validated and widely used in our previous studies [19,20]. To obtain the hot-compressed samples, the liquid sample at 1600 K (approximately 1.2 T_g) was subjected to pressures of 5 GPa, 10 GPa, and 15 GPa, respectively, and maintained at the temperature and pressure for 125 ps to allow for adequate structural relaxation. Subsequently, the samples were cooled at a rate of 1 K/ps to 300 K, after which the pressure is released at a rate of 0.1 GPa/ps. Finally, the sample was relaxed again for 125 ps under zero pressure.

To assess the dependence of Young's modulus (E) and fracture toughness (K_{IC}) on pressure, approximately 650,000 atoms were randomly placed in a slab simulation box (54 × 54 × 3 nm^3). The preparation of the initial sample and hot-compressed samples followed the steps described above. A pre-crack with a length of 15 nm and a tip radius of 0.6 nm was then introduced at the center of the sample thickness. After energy minimization, the pre-crack structure was relaxed for 200 ps at 300 K in an NPT ensemble. The pre-crack structure was then gradually stretched along the crack's perpendicular direction until fracture occurred, with a strain rate of 0.5 nm^{-1}. This process has been widely validated with successful results [21–23]. E was calculated from the stress-strain curve obtained from the stretching simulation by performing a linear fit on data within the strain range of 0–0.5 %. K_{IC} was calculated using the method proposed by Brochard et al. [24]. Specifically, the formula for K_{IC} is $K_{IC}=\sqrt{E \times G_c}$, where $Gc = \frac{L_y L_z}{\Delta A_\infty}\int_0^{\varepsilon_{xx}^f} L_x\sigma_{xx}\, d\varepsilon_{xx}$ is the critical energy release rate, L_x, L_y, and L_z are the dimensions of the initial model in each direction, ΔA_∞ is the new crack surface area formed during crack propagation, ε_{xx}^f is the maximum strain in the x-direction, and σ_{xx} and ε_{xx} are the stress and strain in the stretching direction, respectively. To enhance the reliability of the results, three parallel experiments were performed for each sample to obtain an average value and a standard deviation.

Fig. 1 illustrates the pressure-dependent evolution of density, glass transition temperature (T_g), Young's modulus (E), fracture toughness (K_{IC}), and oxygen tri-clusters ($^{(3)}O$) content in aluminosilicate glasses. The density increases monotonically with pressure (Fig. 1a), with molecular dynamics (MD) simulations showing close agreement with experimental measurements. T_g, determined from the intersection of linear fits to the potential energy-temperature curve (Fig. 1b), rises systematically with pressure, which can be attributed to the reduction in non-bridging oxygen content, indicating enhanced network connectivity [25]. Young's modulus (E) increases with pressure (Fig. 1c), due to the enhanced density, increased network rigidity, and improved medium-range order [11,26–28]. However, the simulated values are lower than experimental data, likely due to structural differences, i.e., lower medium-range order, particularly the absence of paracrystalline structures (discussed further below). Experimentally, K_{IC} increases by 107 % (from 0.96 ± 0.04 MPa·$m^{1/2}$ to 1.99 ± 0.06 MPa·$m^{1/2}$) between 10 and 15 GPa (Fig. 1d), while simulations show deviations above 10 GPa, failing to accurately reflect this trend, likely due to the absence of experimentally observed paracrystalline structures [14]. The inherent limitations of MD—namely, ultrafast cooling rates (~10^{12} K/s) that suppress medium-range order—explain this discrepancy [29]. Notably, Fig. 1(d) also shows that the $^{(3)}O$ content exhibits a trend similar to K_{IC} across the pressure range studied, indicating that $^{(3)}O$ plays a key role in enhancing the K_{IC} of aluminosilicate glasses.

The mechanical response of aluminosilicate glass under pressure

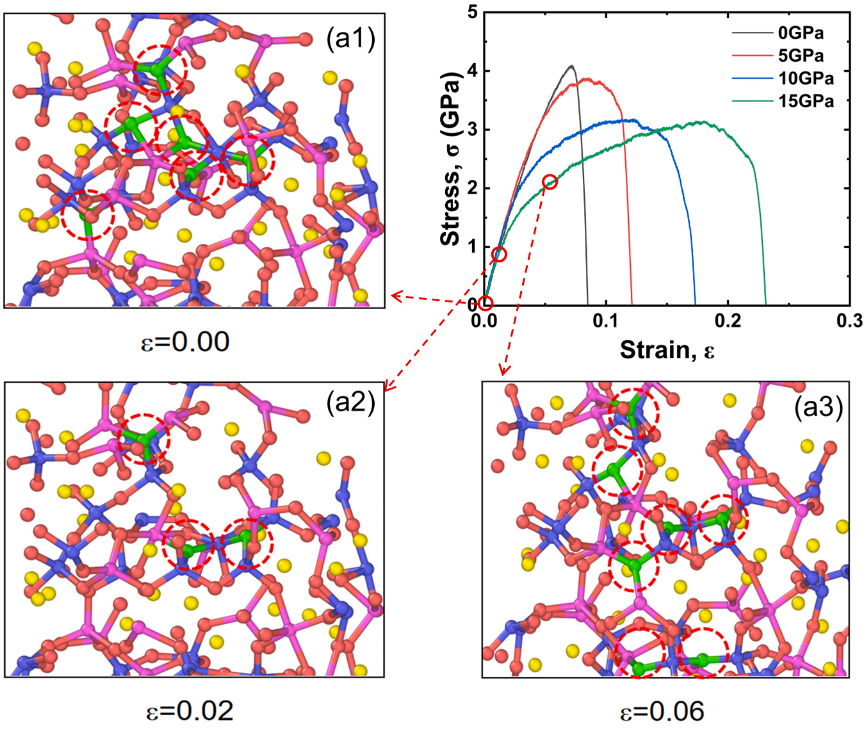

Fig. 2. Stress-strain curves of glass under different pressures. (a1)-(a3) show snapshots of the $^{(3)}$O bond environment changes at ε = 0.00, 0.02, and 0.06, respectively, for glass subjected to hot-compression at 15 GPa. The atoms are colored as follows: oxygen (red and green), silicon (blue), calcium (yellow), and aluminum (pink). The dashed circle (red) indicates $^{(3)}$O.

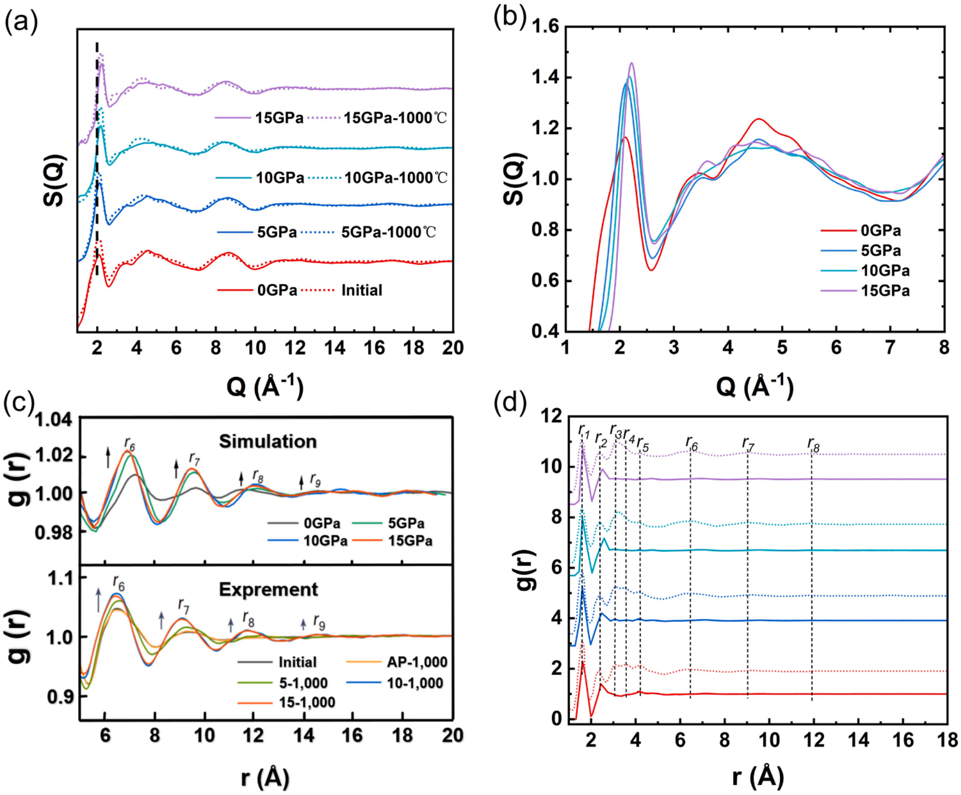

Fig. 3. The distribution of the (a) X-ray scattering structure factor, (b) range (1–8 Å^{-1}) X-ray scattering structure factors of the simulated data, (c) medium-range (5–20 Å) pair distribution function, and (d) pair distribution function of glass under different pressures. Curves in the (a) and (d) with different pressure are shifted in the y-axis for clarity. The data on the breakpoint line and the lower part of (c) are experimental data from Ref [14].

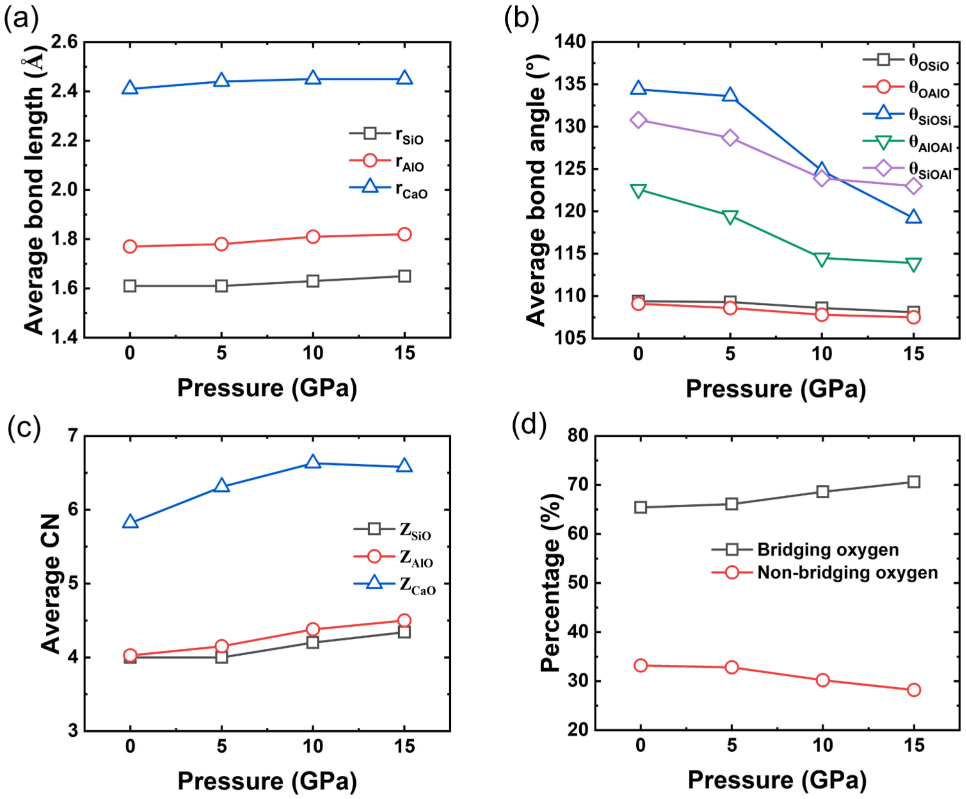

Fig. 4. The distribution of (a) average bond length, (b) average bond angle, (c) average coordination number, and (d) the bridging oxygen and non-bridging oxygen of glass under different pressures. The error bar is less than or equal to the size of the symbol.

varies across both small-strain (elastic) and large-strain regimes. Fig. 2 shows stress-strain (σ-ε) curves at different pressures. The initial uncompressed glass (0 GPa) displays brittle fracture behavior, characterized by a nearly linear σ-ε relationship up to maximum strength, followed by abrupt stress drop without softening (Fig. 2). With increasing pressure, the glass exhibits progressive enhancement in post-yield softening and nano-ductility. Concurrently, fracture toughness (K_{IC}) increases with pressure, aligning with trends reported by Guerette et al. [11]. While our simulations demonstrate clear improvements in K_{IC} and nano-ductility under pressure, they reveal a decrease in fracture strength (peak stress in σ-ε curves) that contrasts with experimental observations [14]. This apparent discrepancy likely attributed to paracrystalline structures, which has been shown to be strengthening phases that are crucial for making the material stronger [14]. Such mesoscale ordered domains are absent in our simulations, hence lacking a mechanism to increase strength. In contrast, the structural reorganization on the local scale, i.e., the formation of $^{(3)}$O might be amplified since this becomes the primary path to densify the glass, in contrast to previous experiments. Such a structural difference may further reduce the strength in the hot-compressed glass sample.

To probe the role of $^{(3)}$O in fracture behavior, we analyzed their bonding dynamics under tensile strain. Fig. 2(a1)-(a3) sequentially capture the evolution of $^{(3)}$O bonding environments in 15 GPa hot-compressed glass during deformation. A distinct bond rupture-reformation cycle is observed for $^{(3)}$O sites during stretching. This dynamic behavior enhances fracture resistance through two synergistic mechanisms: (i) The ionic nature of $^{(3)}$O bonds lowers their activation energy for reorganization compared to covalent Si/Al–O bonds [30], enabling preferential bond switching to dissipate strain energy. (ii) The structural flexibility of $^{(3)}$O facilitates localized shear flow, mitigating stress concentration at crack tips. These findings reconcile with recent reports [31] emphasizing $^{(3)}$O's role in improving toughness and nano-ductility in calcium aluminosilicates. Crucially, the simulations demonstrate that $^{(3)}$O-driven plasticity operates independently of crystallization—no paracrystalline phases were detected, contrasting with experimental interpretations attributing K_{IC} gains to [AlO_6]-rich paracrystalline domains [14]. While $^{(3)}$O may coexist with such domains experimentally, its dynamic behavior here is intrinsically tied to glassy disorder, decoupling its role from crystallization effects. This finding aligns with recent experimental and simulation studies [31,32] confirming the critical role of $^{(3)}$O in toughening calcium aluminosilicate glasses. While simulations show that $^{(3)}$O alone enhances fracture toughness by 33 % from 10 to 15 GPa, the experimental K_{IC} increase of 107 % suggests synergistic contributions from both $^{(3)}$O dynamics and paracrystalline structures—the latter absent in simulations due to ultrafast cooling rates. The spatial correlation between $^{(3)}$O and [AlO_6] sites (Fig. 5b) provides a mechanistic link: $^{(3)}$O may facilitate local structural flexibility and energy dissipation, potentially nucleating paracrystalline domains under experimental conditions. Thus, $^{(3)}$O likely provides a foundational toughening mechanism, which paracrystalline structures further amplify.

To assess pressure-induced structural evolution, Fig. 3 compares simulated and experimental [33] X-ray scattering structure factors (S(Q)) and pair distribution functions (PDFs). The simulated S(Q) peak positions align approximately with experimental data (Fig. 3a). With increasing pressure, the first S(Q) peak shifts to higher Q values (Fig. 3a), consistent with the density increase shown in Fig. 1(a), while its sharpening and intensification (Fig. 3b) suggest enhanced medium-range order (MRO). However, the simulated first peak exhibits lower intensity than experimental results, reflecting reduced MRO in simulations. This discrepancy is more pronounced in the PDF's medium-range region (r_6–r_9, Fig. 3b), where pressure intensifies peak amplitudes, further supporting MRO enhancement. Experimentally, short-range structural changes manifest as sharpened PDF peaks in the r_3–r_5 range (Fig. 3c), a feature absent in simulations. This discrepancy may be attributed to differences in cooling rates, pressurization and/or

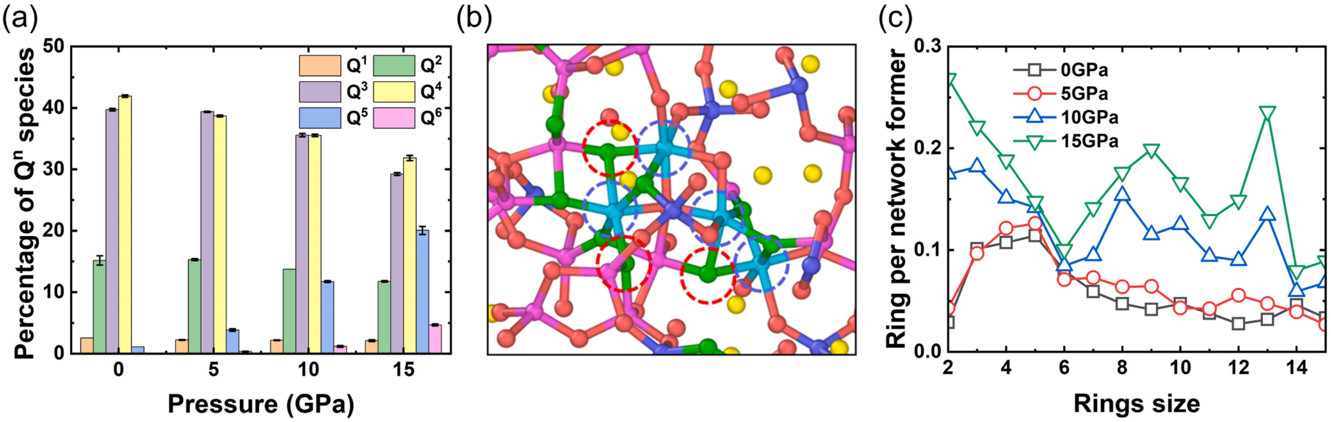

Fig. 5. The distribution of Q^n (a) and ring size (c) in the glass under different pressures. Ring per network former represents the population of rings normalized by the total number of Si and Al. (b) shows a snapshot of the bonding environment of [AlO_6] octahedra and $^{(3)}O$ in the glass subjected to hot-compression at 15 GPa. The atoms are colored as follows: oxygen (red and green), silicon (blue), calcium (yellow), and aluminum (pink and cyan). The dashed circle (red) highlights $^{(3)}O$, and the dashed circle (blue) highlights [AlO_6] octahedra. The error bar is less than or equal to the size of the symbol.

depressurization rates, and other conditions between the experimental and simulation processes.

Fig. 4 summarizes pressure-induced changes in bond lengths, bond angles, coordination numbers (*CN*s), and oxygen speciation (bridging oxygen, *BO*; non-bridging oxygen, *NBO*). The average bond lengths of Si–O, Al–O, and Ca–O show minimal variation with pressure (Fig. 4a), due to the high strength and rigidity of the bonds. Oxygen-centered bond angles decrease significantly under high pressure: Si–O–Si declines from 134.4° to 119.2°, Al–O–Al from 122.6° to 113.9°, and Si–O–Al from 130.8° to 123.0° (Fig. 4b), while tetrahedral O–Si–O and O–Al–O angles remain statistically unchanged, which is consistent with the well-known theory of rigid units in glass (rigid [SiO_4] and [AlO_4] tetrahedra). The *CN*s of Si-O increase from 4.00 to 4.3, Al-O from 4.0 to 4.5, and Ca-O from 5.8 to 6.6 under high pressure (Fig. 4c), respectively. This trend agrees with the nuclear magnetic resonance (NMR) studies of hot-compressed calcium aluminosilicate glasses, including compositions $3CaO$-Al_2O_3–$6SiO_2$ [34] and $41.9CaO$-$18.9Al_2O_3$–$39.2SiO_2$ [35]. Concurrently, the proportion of *BO* (including $^{(3)}O$) rises from 65.4 % to 70.6 %, while *NBO* decreases from 33.2 % to 28.2 % (Fig. 4d). These structural trends align with prior studies [36–40], where permanent densification correlates with reduced oxygen-centered bond angles and increased *CN*s. Notably, the degree of polymerization in the glasses, defined as the ratio of *NBO/T* (*T* refers to the number of four-coordinated network-forming cations, Si and Al), approaches 2.0. This suggests a highly polymerized glass structure with an increase in viscosity under high pressure as stated by a previous study [41].

Beyond short-range order, medium-range structural features evolve under pressure. Fig. 5 presents the changes in Q^n distribution ("n" denotes the number of bridging oxygens per network-forming atom) and ring size distribution. In the initial uncompressed glass, Q^3 and Q^4 dominate, with minor Q^2 and negligible Q^5. Pressure reduces Q^2~Q^4 proportions while increasing Q^5 and Q^6, consistent with the observed decline in *NBO* content and rise in density, *CN*s, and *BO* content (Figs. 1a and 4c-d). The [AlO_6] octahedra structure [14] is also observed in the simulation, which accounts for 5.3 % of total Al. All Al in [AlO_6] are associated with $^{(3)}O$ (Fig. 5b), though the majority of $^{(3)}O$ remains linked to [SiO_4], [SiO_5], [AlO_4], and [AlO_5]. In addition, Ring size analysis (primitive ring criterion [42]) reveals a broad distribution (Fig. 5c). Pressure increases small rings ($n \leq 4$) but also elevates intermediate ($n = 5$–7) and large ($n \geq 8$) rings, particularly above 10 GPa. The simultaneous proliferation of all rings under pressure indicates structural heterogeneity increases with densification. This counterintuitive trend—enhanced MRO coexisting with ring size diversification—highlights the complex interplay between network polymerization and topological disorder.

In conclusion, this study elucidates the interplay between hot-compression, structural evolution, and mechanical enhancement in calcium aluminosilicate glass. The observed improvements in stiffness (E), fracture toughness (K_{IC}), and nano-ductility under pressure appear to arise from two complementary structural mechanisms:

- Dynamic $^{(3)}O$ bonding behavior: The reversible rupture-reformation cycle of $^{(3)}O$ bonds promotes energy dissipation and shear accommodation, directly enhancing K_{IC} and nano-ductility.
- Network polymerization: Pressure-driven conversion of Q^2-Q^4 to Q^5 and Q^6 species and increased C*N*s amplify network connectivity and MRO, indirectly improving stiffness (E) and thermal stability (T_g).

Notably, the co-occurrence of $^{(3)}O$ dynamics and Q^5/Q^6 formation suggests these processes are intertwined rather than independent. While MD simulations indicate that $^{(3)}O$-driven plasticity can operate without paracrystalline phases, experimental observations of [AlO_6]-rich domains highlight the need to reconcile glassy disorder and incipient ordering under high pressure.

The pressure-induced broadening of ring size distributions further implies that densification may amplify structural heterogeneity—a counterintuitive finding that merits deeper exploration. These insights tentatively suggest that optimizing $^{(3)}O$ populations and network connectivity could improve glass performance via pressure processing, though practical applications will require balancing competing structural effects. Future work should address MD-experimental discrepancies in K_{IC} trends and probe the universality of $^{(3)}O$ mechanics across glass compositions.

CRediT authorship contribution statement

Ziming Yan: Writing – review & editing, Writing – original draft, Visualization, Validation, Formal analysis, Data curation. **Zhen Zhang:** Writing – review & editing, Writing – original draft, Validation, Methodology, Funding acquisition, Formal analysis. **Madoka Ono:** Writing – review & editing, Validation, Methodology, Investigation, Formal analysis. **Juanjuan Zhu:** Writing – review & editing, Validation, Resources, Investigation. **Linfeng Ding:** Writing – review & editing, Writing – original draft, Visualization, Validation, Supervision, Resources, Project administration, Methodology, Investigation, Funding acquisition, Formal analysis, Conceptualization. **Lianjun Wang:** Writing – review & editing, Supervision, Resources, Investigation, Funding acquisition.

Declaration of competing interest

The authors declare that they have no known competing financial interests or personal relationships that could have appeared to influence the work reported in this paper.

Acknowledgements

The authors from China gratefully acknowledge financial support from the National Natural Science Foundation of China (U22A20125, U24A2052, and 12474185) and Fundamental Research Funds for the Central Universities (2232024G-07, 2232025A-03).

References

[1] C.M. Jantzen, Systems approach to nuclear waste glass development, J. Non-Cryst. Solids. 84 (1986) 215–225.

[2] C.M. Jantzen, K.G. Brown, J.B. Pickett, Durable glass for thousands of years, Int. J. Appl. Glass Sci. 1 (2010) 38–62.

[3] E.J. Frankberg, J. Kalikka, F. García Ferré, L. Joly-Pottuz, T. Salminen, J. Hintikka, M. Hokka, S. Koneti, T. Douillard, B.Le Saint, M.J. Cordill, T. Epicier, D. Stauffer, M. Vanazzi, L. Roiban, J. Akola, F.D. Fonzo, E. Levänen, K. Masenelli-Varlot, Highly ductile amorphous oxide at room temperature and high strain rate, Science 366 (2019) 864–869.

[4] X. Yu, T.J. Marks, A. Facchetti, Metal oxides for optoelectronic applications, Nat. Mater. 15 (2016) 383–396.

[5] M. Potuzak, R.C. Welch, J.C. Mauro, Topological origin of stretched exponential relaxation in glass, J. Chem. Phys. 135 (2011) 214502.

[6] M. Potuzak, J.C. Mauro, T.J. Kiczenski, A.J. Ellison, D.C. Allan, Communication: resolving the vibrational and configurational contributions to thermal expansion in isobaric glass-forming systems, J. Chem. Phys. 133 (2010) 091102.

[7] S. Yoshida, A. Hidaka, J. Matsuoka, Crack initiation behavior of sodium aluminosilicate glasses, J. Non-Cryst. Solids. 344 (2004) 37–43.

[8] X. Ke, Z. Shan, Z. Li, Y. Tao, Y. Yue, H. Tao, Toward hard and highly crack resistant magnesium aluminosilicate glasses and transparent glass-ceramics, J. Am. Ceram. Soc. 103 (2020) 3600–3609.

[9] M. Ono, Y. Tanabe, M. Fujioka, H. Yamada, K. Ohara, S. Kohara, M. Fujinami, J. Nishii, Direct observation of the topological pruning in silica glass network; the key for realizing extreme transparency, Nat. Protoc. Asia Mater. 17 (2025) 5.

[10] M. Ono, S. Aoyama, M. Fujinami, S. Ito, Significant suppression of Rayleigh scattering loss in silica glass formed by the compression of its melted phase, Opt. Express. 26 (2018) 7942–7948.

[11] M. Guerette, M.R. Ackerson, J. Thomas, F. Yuan, E. Bruce Watson, D. Walker, L. Huang, Structure and properties of silica glass densified in cold compression and hot compression, Sci. Rep. 5 (2015) 15343.

[12] K.H. Lee, Y. Yang, L. Ding, B. Ziebarth, J.C. Mauro, Effect of pressurization on the fracture toughness of borosilicate glasses, J. Am. Ceram. Soc. 105 (2022) 2536–2545.

[13] H. Tang, X. Yuan, Y. Cheng, H. Fei, F. Liu, T. Liang, Z. Zeng, T. Ishii, M.S. Wang, T. Katsura, Synthesis of paracrystalline diamond, Nature 599 (2021) 605–610.

[14] H. Tang, Y. Cheng, X. Yuan, K. Zhang, A. Kurnosov, Z. Chen, W. Xiao, H. S. Jeppesen, M. Etter, T. Liang, Toughening oxide glasses through paracrystallization, Nat. Mater. 22 (2023) 1189–1195.

[15] S. Sundararaman, L. Huang, S. Ispas, W. Kob, New interaction potentials for borate glasses with mixed network formers, J. Chem. Phys. 152 (2020) 104501.

[16] S. Sundararaman, L. Huang, S. Ispas, W. Kob, New interaction potentials for alkali and alkaline-earth aluminosilicate glasses, J. Chem. Phys. 150 (2019) 154505.

[17] S. Sundararaman, L. Huang, S. Ispas, W. Kob, New optimization scheme to obtain interaction potentials for oxide glasses, J. Chem. Phys. 148 (2018) 194504.

[18] H. Liu, B. Deng, S. Sundararaman, Y. Shi, L. Huang, Understanding the response of aluminosilicate and aluminoborate glasses to sharp contact loading using molecular dynamics simulation, J. Appl. Phys. 128 (2020) 035106.

[19] L. Ding, R. Lu, L. Wang, Q. Zheng, J.C. Mauro, Z. Zhang, Nanoindentation-induced evolution of atomic-level properties in silicate glass: insights from molecular dynamics simulations, J. Am. Ceram. Soc. 107 (2024) 1448–1458.

[20] Z. Yan, R. Lu, L. Ding, L. Wang, Z. Zhang, Distinct deformation mechanisms of silicate glasses under nanoindentation: the critical role of structure, J. Appl. Phys. 136 (2024) 245101.

[21] B. Deng, J. Luo, J.T. Harris, C.M. Smith, M.E. McKenzie, Molecular dynamics simulations on fracture toughness of Al$_2$O$_3$-SiO$_2$ glass-ceramics, Scripta Mater. 162 (2019) 277–280.

[22] T. Du, S.S. Sørensen, Q. Zhou, M. Bauchy, M.M. Smedskjaer, Accessing a forbidden disordered state of a zeolitic imidazolate framework with higher stiffness and toughness through irradiation, Chem. Mater. 34 (2022) 8749–8759.

[23] B. Deng, J. Luo, J.T. Harris, C.M. Smith, M.E. McKenzie, Toughening of Li$_2$O-2SiO$_2$ glass-ceramics induced by intriguing deformation behavior of lithium disilicate nanocrystal, J. Am. Ceram. Soc. 103 (2020) 965–972.

[24] L. Brochard, G. Hantal, H. Laubie, F.J. Ulm, R.J.M. Pellenq, V. Poromechanics, Fracture Mechanisms in Organic-Rich Shales: Role of Kerogen, American Society of Civil Engineers, Vienna, Austria, 2013, pp. 2471–2480.

[25] T.K. Bechgaard, A. Goel, R.E. Youngman, J.C. Mauro, S.J. Rzoska, M. Bockowski, L. R. Jensen, M.M. Smedskjaer, Structure and mechanical properties of compressed sodium aluminosilicate glasses: role of non-bridging oxygens, J. Non-Cryst. Solids. 441 (2016) 49–57.

[26] Y. Xiang, J. Du, M.M. Smedskjaer, J.C. Mauro, Structure and properties of sodium aluminosilicate glasses from molecular dynamics simulations, J. Chem. Phys. 139 (2013) 044507.

[27] S. Lan, L. Zhu, Z. Wu, L. Gu, Q. Zhang, H. Kong, J. Liu, R. Song, S. Liu, G. Sha, Y. Wang, Q. Liu, W. Liu, P. Wang, C.T. Liu, Y. Ren, X.L. Wang, Author correction: a medium-range structure motif linking amorphous and crystalline states, Nat. Mater. 21 (2022) 262.

[28] T. To, S.S. Sorensen, J.F.S. Christensen, R. Christensen, L.R. Jensen, M. Bockowski, M. Bauchy, M.M. Smedskjaer, Bond Switching in, Densified oxide glass enables record-high fracture toughness, ACS Appl. Mater 13 (2021) 17753–17765.

[29] X. Li, W. Song, K. Yang, N. Krishnan, B. Wang, M.M. Smedskjaer, J.C. Mauro, G. Sant, M. Balonis, M. Bauchy, Cooling rate effects in sodium silicate glasses: bridging the gap between molecular dynamics simulations and experiments, J. Chem. Phys. 147 (2017) 074501.

[30] A. Nemukhin, F. Weinhold, Structures of the aluminum oxides studied by ab initio methods with natural bond orbital analysis, J. Chem. Phys. 97 (1992) 3420–3430.

[31] T. Du, Z. Chen, S.M. Johansen, Q. Zhang, Y. Yue, M.M. Smedskjaer, Predicting stiffness and toughness of aluminosilicate glasses using an interpretable machine learning model, Eng. Fract. Mech. 318 (2025) 110961.

[32] Z. Shan, T. Zhao, X. Ke, J. Ren, H. Tao, Y. Yue, Oxygen tri-clusters make glass highly crack-resistant, Acta Mater 262 (2024) 119425.

[33] M.T. Dove, M.G. Tucker, D.A. Keen, Neutron total scattering method: simultaneous determination of long-range and short-range order in disordered materials, Eur. J. Mineral. 14 (2002) 331–348.

[34] J.R. Allwardt, J.F. Stebbins, B.C. Schmidt, D.J. Frost, A.C. Withers, M. M. Hirschmann, Aluminum coordination and the densification of high-pressure aluminosilicate glasses, Am. Mineral 90 (2005) 1218–1222.

[35] R. Muniz, D. De Ligny, C. Martinet, M. Sandrini, A. Medina, J. Rohling, M. Baesso, S. Lima, L. Andrade, Y. Guyot, In situ structural analysis of calcium aluminosilicate glasses under high pressure, J. Phys.: Condens. Matter. 28 (2016) 315402.

[36] D.A. Kilymis, J.M. Delaye, S. Ispas, Behavior of sodium borosilicate glasses under compression using molecular dynamics, J. Chem. Phys. 143 (2015) 094503.

[37] C. Martinet, A. Kassir-Bodon, T. Deschamps, A. Cornet, S.Le Floch, V. Martinez, B. Champagnon, Permanently densified SiO2 glasses: a structural approach, J. Phys. Condens. Matter. 27 (2015) 325401.

[38] D.A. Kilymis, J.M. Delaye, S. Ispas, Nanoindentation of the pristine and irradiated forms of a sodium borosilicate glass: insights from molecular dynamics simulations, J. Chem. Phys. 145 (2016) 044505.

[39] S.K. Lee, P.J. Eng, H.k. Mao, J. Shu, Probing and modeling of pressure-induced coordination transformation in borate glasses: inelastic x-ray scattering study at high pressure, Phys. Rev. B. 78 (2008) 214203.

[40] M.M. Smedskjaer, R.E. Youngman, S. Striepe, M. Potuzak, U. Bauer, J. Deubener, H. Behrens, J.C. Mauro, Y. Yue, Irreversibility of pressure induced boron speciation change in glass, Sci. Rep. 4 (2014) 3770.

[41] Y. Wang, T. Sakamaki, L.B. Skinner, Z. Jing, T. Yu, Y. Kono, C. Park, G. Shen, M. L. Rivers, S.R. Sutton, Atomistic insight into viscosity and density of silicate melts under pressure, Nat. Commun. 5 (2014) 3241.

[42] K. Goetzke, H.J. Klein, Properties and efficient algorithmic determination of different classes of rings in finite and infinite polyhedral networks, J. Non-Cryst. Solids. 127 (1991) 215–220.